Ray, L., Förster, H.-J., Förster, A., Fuchs, S., Naumann, R., Appelt, O. (2015): Tracking the thermal properties of the lower continental crust: Measured versus calculated thermal conductivity of high-grade metamorphic rocks (Southern Granulite Province, India). - *Geothermics*, *55*, p. 138-149.

DOI: http://doi.org/10.1016/j.geothermics.2015.01.007

Tracking the thermal properties of the lower continental crust: measured versus calculated thermal conductivity of high-grade metamorphic rocks (Southern Granulite Province, India)

This paper was originally published in:

Geothermics [Elsevier], Mar 2015,

doi: 10.1016/j.geothermics.2015.01.007

The final publication is available at:

http://link.springer.com/article/10.1007%2Fs12665-013-2679-2

Received: 18.04.2014
Accepted: 19.01.2015
Published online: 10.03.2015

Authors

Labani Ray, Hans-Jürgen Förster, Andrea Förster, Sven Fuchs, Rudolf Naumann, Oona Appelt

Affiliations

Labani Ray (corresponding author)
CSIR-National Geophysical Research Institute, Uppal Road, Hyderabad 500007, India
Tel.: +91 40 27012385, Fax: +91 40 23434651, E-mail: labani@ngri.res.in

L. Ray, CSIR-National Geophysical Research Institute, Uppal Road, Hyderabad 500007, India
H.-J. Förster, GeoForschungsZentrum Potsdam (GFZ), Telegrafenberg, D-14773, Potsdam, Germany
A. Förster, GeoForschungsZentrum Potsdam (GFZ), Telegrafenberg, D-14773, Potsdam, Germany
S. Fuchs, Aarhus University, Høegh-Guldbergs Gade 2, 8000 Aarhus C, Denmark
R. Naumann, GeoForschungsZentrum Potsdam (GFZ), Telegrafenberg, D-14773, Potsdam, Germany
O. Appelt, GeoForschungsZentrum Potsdam (GFZ), Telegrafenberg, D-14773, Potsdam, Germany

Abstract

In this study, the bulk thermal conductivity (TC) of 26 rock samples representing different types of granulite-facies rocks, *i.e.* felsic, intermediate and mafic granulites, from the Southern Granulite Province, India is measured at dry and saturated conditions with the optical-scanning method.

Thermal conductivity also is calculated from modal mineralogy (determined by XRD and EPMA), applying several mixing models commonly used in thermal studies. Most rocks are fine- to medium -grained equigranular in texture. All samples are isotropic to weakly anisotropic and possess low porosities (< 2%). Measured TC values range between 2.5 and 3.0 W m^{-1} K^{-1} for felsic granulites, between 2.5 and 3.5 W m^{-1} K^{-1} for intermediate granulites and between 2.4 and 2.7 W m^{-1} K^{-1} for mafic granulites. Considering this data and literature compilations, rocks representative for the lower continental crust typically display values between 2 and 3 W m^{-1} K^{-1} at ambient temperature and pressure conditions. Depending on the mixing model and the mineral TC value used in the calculations, measured and calculated bulk TC could be properly fitted. For mean values of mineral TCs, the harmonic mean provides an almost perfect fit, with a mean deviation of $-1 \pm 6\%$ (1σ). However, the implication of that correspondence would be that minerals and pores are predominantly aligned parallel, which is in apparent contrast to the texture of the rocks studied here. The geometric mean, which does not consider any layering of minerals or pores in the rock and, thus, should be in better harmony with the textural characteristics of the studied high-grade rocks, matches the measured TC data very well, if minimal minerals TCs reported in the literature are applied (mean deviation $5 \pm 8\%$). In case of non-availability of If appropriate samples (in terms of sample size or physical-chemical-mechanical condition) for laboratory measurement are not available, bulk TC of high-grade metamorphic rocks with low anisotropy and porosity could be satisfactorily good assessed from modal mineralogy, using the data sets for mineral TC applied in this study. Further work is required on the applicability of mixing models to compute TC of other rock types, *e.g.*, of igneous and sedimentary rocks.

Keywords: 3D geological model, conductive thermal field, coupled fluid and heat transport, Energy Atlas Berlin

Highlights

- Bulk thermal conductivity (TC) of granulites is measured by optical-scanning method (85)
- Mineralogical composition of these rocks is determined by XRD and EPMA (72)
- Bulk TC is calculated from modal mineralogy using various mixing models (74)
- TC of minerals play a vital role in the calculation of bulk TC (64)
- TC at ambient condition for lower crustal rocks ranges between 2 and 3 W m^{-1} K^{-1} (82)

1 Introduction

Thermal conductivity (TC, λ) of rocks is one of the essential thermophysical parameters that govern the thermal structure of the earth. Especially the TC of granulite-facies rocks, representative of the lower continental crust, provides an important constraint on the temperature distribution of the lithosphere. Yet established significant variation of TC in high-grade metamorphic rocks also exerts a major control on the distribution of heat in the lower crust itself. Thus, knowledge on TC of the lower crust is vital in any state-of-the-art thermal-lithosphere study.

Most thermal models are confronted with the problem that TC data for the lower crust are not available for a study area and literature-data need to be considered. Thermal conductivity is generally measured in the laboratory on core or outcrop rock samples. However, lower-crustal lithologies are only rarely exposed in surface outcrops or by drillcore, which would permit to determine TC values directly in the laboratory. In some places, probes of the lower crust are brought up to the surface as xenoliths in mafic magmas. These xenoliths, however, are generally small in size, have interacted with the basaltic host magma, experienced metasomatic alteration, or have already undergone surface weathering. All these features hamper or even preclude obtaining reliable TC data by laboratory measurement. (*cf.* Förster *et al.*, 2007).

The TC of a rock is primarily controlled by its mineralogy. Therefore, if appropriate rock samples are not available for direct laboratory measurement, TC may be alternatively assessed by indirect methods, *e.g.*, calculated from the mineral composition of the rock. Fortunately, the size of lower-crustal xenoliths is usually sufficiently large so that their modal mineralogy can be precisely determined, for instance, by X-ray diffraction combined with electron-microprobe analysis. Even if xenoliths are metasomatically overprinted and their original mineralogical composition changed during uprise from their source, the *in-situ* modal mineralogy could be properly reconstructed if the mineral reactions involving the alteration species are known.

Several attempts have been made in the past to calculate the TC of rocks indirectly from its mineral composition (*e.g.*, Birch and Clark, 1940; Beck and Beck, 1965; Horai and Baldridge, 1972; Brigaud and Vasseur, 1989; Pribnow *et al.*, 1993; Pribnow and Umsonst, 1993; Jessop, 2013; Fuchs *et al.*, 2013). All these approaches, however, were confronted with various shortcomings. They involved either only a limited amount of samples, did not consider all common mixing models (see below) or missed the comprehensive mineralogical/geochemical sample characterization. Calculation of rock TC from modal mineralogy is not simple and must further consider the complexity of rock structure/texture. To tackle this problem, several petrophysical models can be applied. These models consider a rock as an n-phase system consisting of minerals and pores. They differ with regard to what they reflect, *e.g.* whether minerals or pores are aligned parallel or

perpendicular to the direction of measurement, resulting in a TC for both directions represented by the arithmetic mean and harmonic mean, respectively. Rock TC can also be assessed considering other mixing models, *e.g.*, the geometric mean (Lichtenecker, 1924), the Hashin-Shtrikman mean (Hashin and Shtrikman, 1962), or the effective-medium mean (Bruggeman, 1935). A comprehensive overview on such mixing models is provided by Abdulagatova *et al.* (2009).

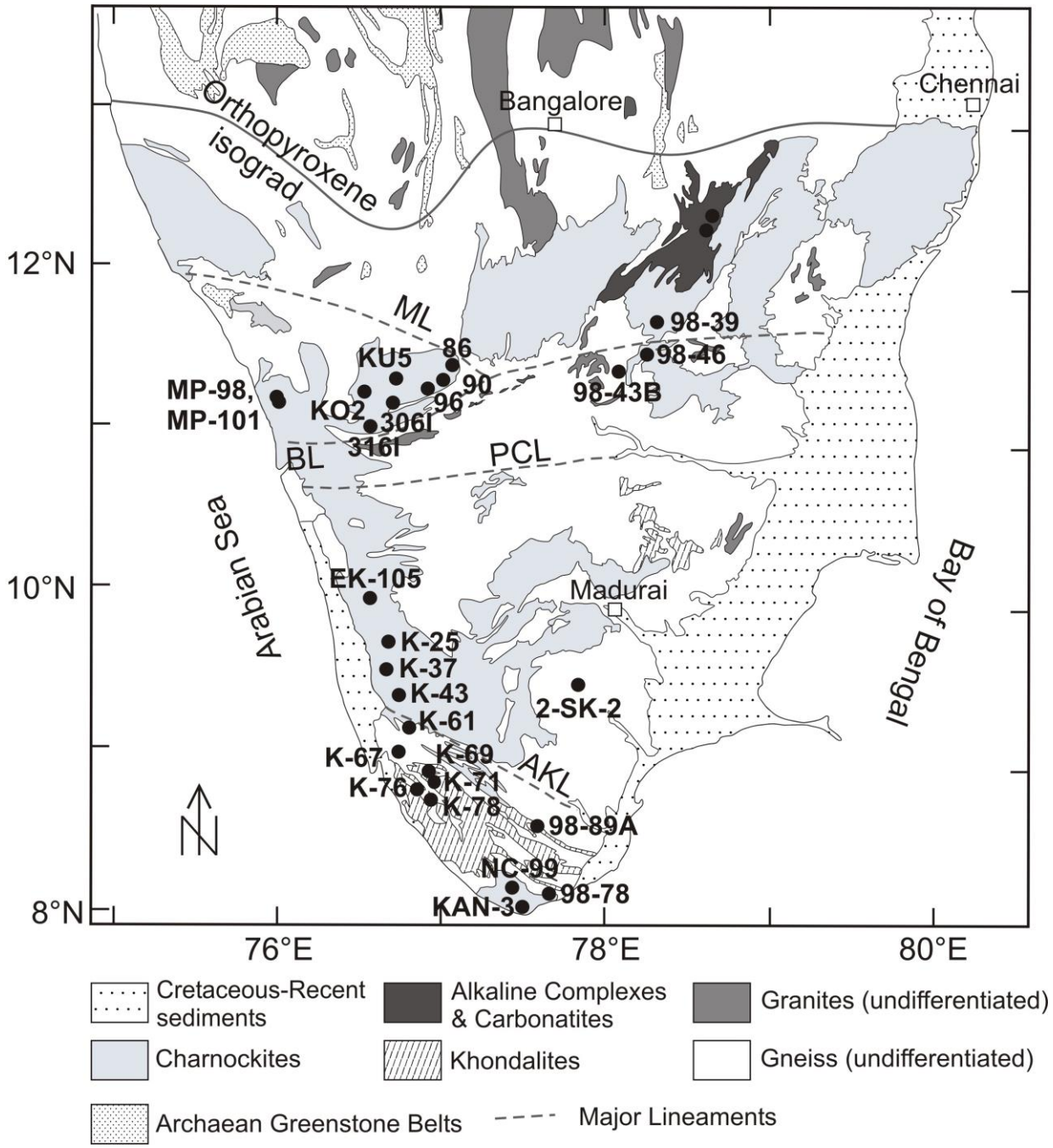

Figure 1: Geological sketch map of the Southern Granulite Province, India (modified after Geological map of India, 1998). Sample locations are shown by solid circles.

The aim of the present study is two-fold. First, it examines whether the indirect determination of rock TC from modal mineralogy may serve as a reliable substitute for laboratory-measured values and what errors are inherent in such an approach. Second, it adds a set of newly measured TC values to the poor database yet existing for the lower crust, demonstrating that the range in TC of this part of the lithosphere may be enormous. In addition to the paucity in values, there are only few studies in which measured TC values for lower-crustal rocks are referred to samples that are also properly characterized petrologically (*cf.* Kukkonen *et al.*, 1999). In our study, full and state-of-the-art mineralogical and geochemical data are provided for all samples.

Our study encompasses a total of 26 fresh, usually fine- to medium-grained equigranular surface rock samples, including eight felsic granulites (charnockites), ten intermediate granulites (enderbites), four mafic granulites and, for comparison, four coarser-grained amphibolite-facies ortho- and paragneisses from the Southern Granulite Province, India (Fig. 1).The sampling area represents one of the largest Precambrian granulite provinces of the world, extending over an area of ~40,000 km^2 (Gopalkrishna *et al.*, 1986). On these samples, (i) measurements of bulk thermal conductivity were conducted using the optical-scanning method, (ii) modal mineralogy and mineral compositions were determined by X-ray diffraction (XRD) and electron-probe microanalysis (EPMA) and (iii) bulk TC values were calculated from mineral data and measured porosity applying common mixing models. Finally (iv), the best-fitting mixing model was delineated, given by the amount of deviation between measured and calculated TC.

2. Analytical methods

2.1. Thermal conductivity and porosity

In principle, three analytical methods are widely in use to perform laboratory TC measurements: (i) the steady-state divided-bar method (*e.g.*, Bullard, 1939; Birch, 1950), (ii) the transient line-source method (*e.g.*, Carslaw and Jaeger, 1947; Jaeger, 1958) and (iii) the transient optical-scanning method (*e.g.*, Popov *et al.*, 1999). A comparison of these methods on amphibolite-facies metamorphic rocks revealed a satisfactorily good agreement within the limits of error (Popov *et al.*, 1999).

In this study, TC measurements were performed with the optical-scanning method. The measurement errors, estimated from tests on standards, ranged between 1 and 3%, thus confirming previous estimates for this analytical technique (*cf.* Popov *et al.*, 1999). To check for the reliability of the analytical method applied, a subset of the same samples were additionally measured for TC

by the divided-bar at NGRI (Hyderabad). Both techniques yielded corresponding results within the limits of analytical error.

Measurements were conducted on sawed samples with smooth surfaces that were commonly between 5 and 9 cm in length, 4 and 6 cm in width and 4 and 6 cm in thickness. The TC was measured on both dry and water-saturated rock samples as well as along two directions which were oriented perpendicular to each other. In the situation of a gentle foliation, samples were measured parallel (λ_{PAR}) and perpendicular (λ_{PER}) to the metamorphic texture. For all samples, measurements were performed along 1 to 8 different scanning lines on each direction, with one scanning per line. For each direction, minimum and maximum TC values (averaged from the bulk of scanning line data) were calculated, designated as λ_{MIN} and λ_{MAX}. The respective mean values are denoted as $\lambda_{AVERAGE}$.

Anisotropy (A) of TC in a sample is expressed as

$$A = \frac{\lambda_{PAR}}{\lambda_{PER}} . \quad (1)$$

For each direction, the inhomogeneity factor (ε), reflecting the variability in TC (as function of mineral TC and TC of the pore fluid) was determined by

$$\varepsilon = \frac{\lambda_{MAX} - \lambda_{MIN}}{\lambda_{AVERAGE}} \quad (2)$$

where λ_{MAX}, λ_{MIN} and $\lambda_{AVERAGE}$ are maximum, minimum and average TC.

Porosity was determined using the Archimedes principle by measuring the weight of rock in dry and saturated condition. Dry weight of each sample has been measured after heating the sample in an oven at 100^{o}C for one day. The dry sample has been placed in an evacuated chamber and saturated in distilled water for two to three days. At that time, full saturation was accomplished, controlled by weight measurements.

Data on bulk TC, inhomogeneity, anisotropy and porosity of the studied samples are compiled in Table 1.

2.2. Modal mineralogy and mineral chemistry

Sample powders and polished thin sections were prepared from those samples on which the measurements of thermal conductivity and other petro-physical parameters were conducted, *i.e.*, all data for a sample were acquired from the same specimen.

Table 1 Measured bulk thermal conductivity (saturated), inhomogeneity, anisotropy, and porosity of granulites and gneisses from the Southern Granulite Province, India.

Rock type/ Sample No.	Thermal Conductivity													Porosity
	λ_{PAR} ($Wm^{-1} K^{-1}$)					λ_{PER} ($Wm^{-1} K^{-1}$)					Anisotropy	Mean (λ_m)		(%)
	Range	Av.	SD	ε	n	Range	Av.	SD	ε	n	($\lambda_{PAR}/\lambda_{PER}$)	Av.	SD	
Charnockite														
EK-105	2.43 – 2.94	2.63	0.10	0.15	4	2.35 – 2.95	2.61	0.12	0.18	4	1.01	2.62	0.03	1.3
K-25	2.53 – 2.97	2.79	0.10	0.13	4	2.58 – 2.96	2.77	0.07	0.09	6	1.01	2.78	0.04	0.9
K-37	2.30 – 2.78	2.50	0.10	0.14	6	2.27 – 2.86	2.49	0.11	0.15	4	1.01	2.50	0.04	0.8
K-61	2.52 – 3.01	2.76	0.09	0.13	8	2.48 – 2.98	2.70		0.14	1	1.02	2.76		0.5
K-69	2.43 – 3.59	2.96	0.24	0.30	4	2.36 – 3.59	2.96	0.32	0.37	3	1.00	2.96	0.06	1.3
2-SK-2	2.34 – 2.73	2.47	0.06	0.10	5	2.29 – 2.58	2.43	0.04	0.08	5	1.04	2.45	0.04	0.5
KAN-3	2.54 – 3.33	2.85	0.15	0.22	5	2.47 – 3.08	2.78	0.12	0.17	5	1.03	2.81	0.08	0.7
NC-99	2.53 – 3.22	2.83	0.16	0.20	4	2.40 – 2.92	2.68	0.13	0.18	3	1.06	2.77	0.09	1.4
Enderbite														
98-46	2.46 – 3.09	2.77	0.12	0.16	4	2.40 – 3.16	2.73	0.14	0.20	4	1.01	2.75	0.06	0.7
KU5	2.61 – 4.11	3.52	0.23	0.27	8	2.71 – 4.19	3.53	0.25	0.33	7	1.00	3.53	0.03	1.0
86	2.78 – 3.36	3.05	0.14	0.15	7	2.59 – 3.27	2.97	0.13	0.16	5	1.03	3.02	0.06	0.7
90	2.84 – 4.27	3.56	0.39	0.37	7	3.12 – 4.16	3.47	0.18	0.22	7	1.03	3.51	0.07	1.0
96	2.95 – 3.50	3.20	0.10	0.13	8	2.88 – 3.40	3.11	0.10	0.13	8	1.03	3.15	0.05	0.3
MP-98	2.86 – 3.46	3.23	0.11	0.13	4	2.90 – 3.44	3.22	0.09	0.13	4	1.00	3.22	0.03	0.6
MP-101	2.78 – 3.24	3.00		0.18	1	2.80 – 3.10	2.93		0.17	1	1.02	2.96	0.00	0.2
98-78	2.02 – 2.88	2.55	0.14	0.20	5	2.16 – 2.83	2.50	0.15	0.21	4	1.02	2.52	0.13	0.9
98-89A	2.63 – 3.10	2.82	0.10	0.15	3	2.38 – 3.19	2.77	0.19	0.25	4	1.01	2.79	0.06	1.2
K-71[a]	1.97 – 3.68	2.73	0.58	0.61	3	1.92 – 3.79	2.60	0.64	0.67	3	1.05	2.66	0.07	1.4
Mafic granulite														
98-39	2.15 – 2.95	2.64	0.41	0.54	4	2.18 – 2.68	2.41	0.10	0.15	4	1.08	2.53	0.13	0.7
306I	2.18 – 2.48	2.27	0.07	0.11	8	2.21 – 2.35	2.25	0.04	0.08	5	1.01	2.26	0.03	0.3
316I	2.59 – 2.97	2.81	0.07	0.12	7	2.39 – 2.75	2.57	0.11	0.14	8	1.08	2.68	0.13	1.1
KO2	2.41 – 2.80	2.59	0.08	0.12	8	2.31 – 2.71	2.54	0.06	0.11	6	1.02	2.57	0.04	0.4
Gneiss														
98-43B[b]	1.83 – 2.55	2.30		0.25	1	1.81 – 2.47	2.19		0.25	1	1.05	2.25		1.3
K-78[c]	2.31 – 3.47	3.00		0.35	1	2.34 – 3.23	2.80		0.33	1	1.07	2.90		1.4
K-67[c]	2.50 – 3.65	3.07	0.29	0.31	3	2.39 – 3.27	2.85	0.26	0.30	5	1.06	2.93	0.12	1.3
K-76[c]	2.21 – 3.02	2.79	0.16	0.21	6	2.03 – 2.97	2.60	0.12	0.17	4	1.07	2.71	0.12	1.2

[a] charno-enderbite, [b] paragneiss, [c] orthogneiss, SD = 1δ standard deviation of the TC averages (av.), ε = average of inhomogeneity factor, n = number of measured lines.

Modal mineralogy was determined by X-ray diffraction on powdered samples (< 32µm). Powder X-ray patterns were collected using a PANalytical Empyrean powder diffractometer with Cu Kα radiation, automatic divergent and antiscatter slits and a PIXcel^{3D} detector. The diffraction data were recorded from 5° to 85° 2Θ via a continuous scan with a step-size of 0.0131 and a scan time of 60 s per step.

The generator settings were 40 kV and 40 mA. The Rietveld algorithm BGMN was used for quantitative analysis (Bergmann *et al.*, 1998). Weight percentages were transferred into volume percentages using well established mineral-density values.

To ascertain the mineralogy as comprehensive and accurate as possible, minerals constituting solid solutions were additionally studied by electron microprobe using polished thin sections. The compositions of garnet, pyroxene, amphibole, mica and feldspar were determined using a Cameca SX-100 microprobe operating in the wavelength-dispersive mode. The analytical conditions involved an accelerating voltage of 15 kV, a beam current of 20 nA and a beam size of 5-10 µm. In general, in every thin section, 10 spot analyses were conducted on each of these species and subsequently averaged. All minerals measured were established displaying a high degree of compositional homogeneity, justifying the use of average compositions for calculation of end-members. Thermal-conductivity values of these end-members are listed in Table 2 and subsequently used to calculate rock TC (Table 3).

2.3. Whole-rock geochemistry

Whole-rock geochemical data were obtained from homogenized rock powders < 63µm in size and are tabulated in the Appendix. The major elements and some trace elements (Sc, V, Cr, Ni, Zn and Ga) were determined by wavelength-dispersion X-ray fluorescence spectrometry (XRF) using fused lithium tetraborate discs. All XRF analyses were made with an automated Siemens SRS303AS spectrometer. Total water and CO_2 were determined by combustion - infrared detection. The rare earth elements (REE) plus Rb, Sr, Y, Zr, Nb, Cs, Ba, Hf, Ta, Pb, Th and U were analyzed by inductively coupled plasma-mass spectrometry (ICP-MS; Perkin-Elmer/Sciex Elan Model 500). Details on the analytical procedures are provided in Förster *et al.* (1999).

3. Background on mixing models

Common models for n-phase systems consider a layered arrangement of minerals, with the layer thickness proportional to the volume faction. If λ_i is TC and X_i is the volume fraction of the i-th mineral, *i.e.*, $\sum_{i=1}^{n} X_i = 1$, the **arithmetic mean** (λ_{AM}) and the **harmonic mean** (λ_{HM}) are defined as follows:

$$\lambda_{AM} = \lambda_{BC}^{U} = \sum_{i=1}^{n} X_i \lambda_i \qquad (3)$$

$$\lambda_{HM} = \lambda_{BC}^{L} = \left(\sum_{i=1}^{n} \frac{X_i}{\lambda_i} \right)^{-1} \quad (4)$$

These means, introduced by Voigt (1928) and Reuss (1929), considering mineral arrangements in parallel and perpendicular direction, provide the upper limit (λ_{BC}^{U}) and the lower limit (λ_{BC}^{L}) of TC, respectively. These limits are the so-called Wiener Boundaries after Wiener (1912).

TC can also be estimated using the **geometric-mean** model, which went back to Lichtenecker (1924) and is defined as follows

$$\lambda_{GEO} = \prod_{i=1}^{n} \lambda_i^{Xi} \quad (5)$$

The **Hashin-Shtrikman mean** λ_{HS} (Hashin and Shtrikman, 1962) is the average of the upper bound (λ_{HS}^{U}) and the lower bound (λ_{HS}^{L}) TC of an n-phase isotropic system. The relations are

$$\lambda_{HS}^{U} = \lambda_{\max} + \frac{A_{\max}}{1 - \alpha_{\max} A_{\max}}, \quad (6)$$

$$\lambda_{HS}^{L} = \lambda_{\min} + \frac{A_{\min}}{1 - \alpha_{\min} A_{\min}}, \quad (7)$$

where $\lambda_{\max} = \max(\lambda_1 \ldots\ldots\ldots \lambda_i)$, $\alpha_{\max} = \frac{1}{3\lambda_{\max}}$, $A_{\max} = \sum_{i=1}^{n} \frac{X_i}{\alpha_{\max} + 1/(\lambda_i - \lambda_{\max})}$,

$\lambda_{\min} = \min(\lambda_1 \ldots\ldots\ldots \lambda_i)$, $\alpha_{\min} = \frac{1}{3\lambda_{\min}}$, $A_{\min} = \sum_{i=1}^{n} \frac{X_i}{\alpha_{\min} + 1/(\lambda_i - \lambda_{\min})}$.

In addition, in case of macroscopically homogeneous and isotropic rocks which consist of randomly distributed grains and pores, TC can be estimated from the **effective-medium** theory mean (Bruggeman, 1935) as follows

$$\lambda_{EFF} = 1 \Big/ \left(\sum_{i=1}^{n} \frac{3X_i}{2\lambda + \lambda_i} \right) \quad (8)$$

4. Results

4.1 Measured thermal conductivity

Bulk thermal-conductivity data measured in parallel and perpendicular directions on saturated samples are listed in Table 1. Anisotropy (*A*) of TC, determined by using Eq. (1), is generally low, ranging between 1.01 and 1.08 (Table 1). Average values along each direction (*i.e.*, λ_{PAR}, λ_{PER}) are

shown in Fig. 2. All data points plot below $\lambda_{PAR}/\lambda_{PER}$ = 1, indicating that λ_{PAR} is slightly, but statistically significantly larger than λ_{PER} (paired sample *t*-test, p = 0.001). The low anisotropy revealed by TC measurements indicates that the studied rocks in general are isotropic in nature. The means of anisotropy between the different rock groups are statistically indistinguishable (ANOVA, p = 0.058). Mean bulk TC (λ_M) ranges between 2.5 and 3.0 W m^{-1} K^{-1} for charnockites, between 2.5 and 3.6 W m^{-1} K^{-1} for enderbites and between 2.3 and 2.8 W m^{-1} K^{-1} for mafic granulites (*cf.* Table 1). The gneisses fall in the range 2.3 – 3.1 W m^{-1} K^{-1}. In decreasing order, measured TC averages (± 1σ standard deviation) to 2.72 ± 0.17 W m^{-1} K^{-1} for charnockite, to 3.04 ± 0.34 W m^{-1} K^{-1} for enderbite, to 2.58 ± 0.22 W m^{-1} K^{-1} for mafic granulite, and to 2.79 ± 0.35 W m^{-1} K^{-1} for gneiss, respectively (Fig. 3).

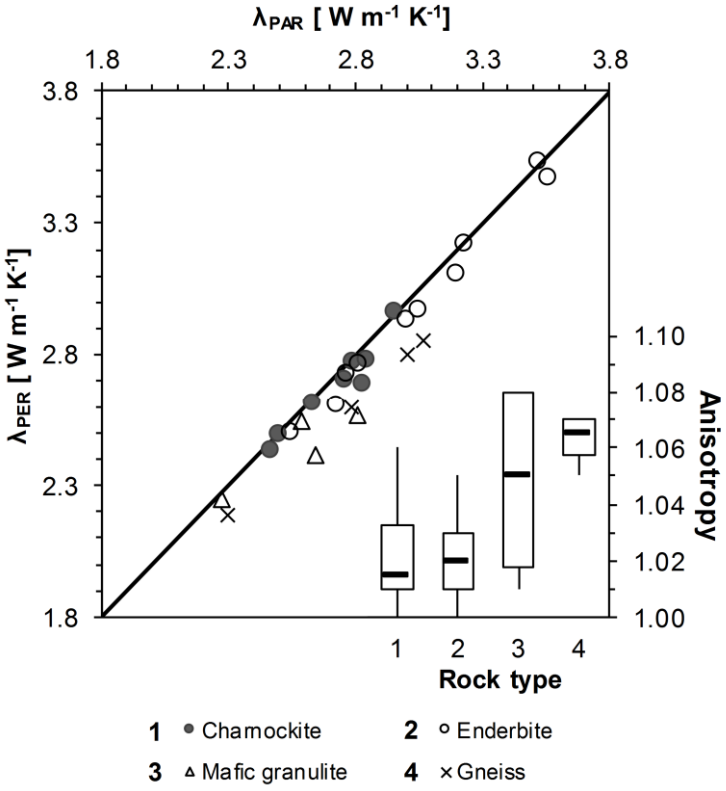

Figure 2: Thermal-conductivity anisotropy of granulites and gneisses illustrated by a scatter plot of bulk water-saturated TC measured perpendicular (λ_{PER}) and parallel to metamorphic fabric (λ_{PAR}) (see text for explanation). Range of anisotropy is shown as box-whisker plot: the box is defined by the lower quartile (25th percentile) and by the upper quartile (75th percentile), the whiskers are defined by the minimum and maximum values observed, the black line is the median value.

The inhomogeneity factor (ε) of most samples amounts to > 0.2 in either parallel or perpendicular direction (Table 1), reflecting the relatively homogeneous nature of the samples in terms of mineralogical variation and porosity distribution. Maximum inhomogeneity is recorded in enderbite sample K-71, which exhibits a factor ε ranging between 0.61 and 0.67 in both directions.

Table 2 Volume percentages of mineral phases/end-members and their thermal conductivities.

Mineral group	Phases or end-members	Mineral TC			Charnockite								Mafic Granulite			
		min	mean	max	EK-105	K-25	K-37	K-61	K-69	2-SK-2	KAN-3	NC-99	98-39	306I	316I	KO2
		($Wm^{-1}K^{-1}$)			(%)	(%)	(%)	(%)	(%)	(%)	(%)	(%)	(%)	(%)	(%)	(%)
	Quartz	7.20[1]	7.69[2]	7.99[1]	25.4	23.8	18.2	32.8	30.5	21.6	33.7	31.1	13.8	1.3	17.2	0.0
Plagioclase	Albite	2.00[3]	2.32[4]	2.35[3]	31.7	23.7	23.4	18.9	18.9	23.9	31.9	36.6	41.8	29.2	15.8	16.5
	Anorthite	1.54[3]	1.68[2]	1.90[5]	10.0	7.6	9.3	11.9	7.7	15.2	13.0	11.6	16.9	18.5	18.4	15.7
	Orthoclase	2.25[3]	2.32[6]	2.68[4]												
K-Feldspar	Orthoclase	2.25[3]	2.32[6]	2.68[4]	21.7	29.4[c]	31.7[c]	19.3	29.2	21.4	15.8	13.9			1.1	
	Albite	2.00[3]	2.32[4]	2.35[3]	5.3	7.1	10.3	2.1	3.7	5.2	2.7	3.4			0.1	
Amphibole	Hornblende	2.54[2]	2.81[3]	3.08[3]	5.1					5.9				11.5	1.4	13.3[e]
Opx	Enstatite	4.12[2]	4.16[a,3]	4.96[2]	0.8	2.8	0.8	0.9	0.9	2.4	0.8	0.8	14.9	7.3	1.3	9.0
	Ferrosilite		4.16[a,3]			4.6				4.5		1.5	8.0	3.9	0.8	12.3
Cpx	Diopside		4.06[3]	4.11[2]			0.4							17.1	19.0	
	Hedenbergite		3.82[b,3]				2.4							6.5	5.6	
	Clinoferrosilite		3.82[b,3]				0.8							1.9	2.9	
	Jadeite		4.62[3]	6.66[2]										1.6	1.4	
Garnet	Almandine		3.31[2]					2.7	3.5				1.8		6.3	10.7
	Pyrope		3.18[2]					2.4	2.9				1.5		3.5	10.5
	Grossular	5.12[2]	5.48[3]	5.64[2]											2.8	
Mica	Biotite	1.95[5]	2.02[3]	2.34[2]		0.4		8.3	1.7		2.1	0.3				
	Phlogopite	1.963	2.13[3]	2.29[2]												12.1
Others	Illite	1.85[7]	1.90[8]	2.00[9]											2.6	
	Ilmenite	2.19[2]	2.38[3]			0.5	0.7	0.8	1.2			0.8	1.4			
	Magnetite	5.10[2]	5.11[3]	5.84[3]			1.9							1.1[d]		
	Epidote	2.62[2]	2.84[3]	3.03[3]												

Continued

Mineral group	Phases or end-members	Mineral TC			Enderbite										Gneiss			
		min	mean	max	98-46	KU-5	86	90	96	MP-98	MP-101	98-78	98-89A	K-71	98-43B	K-78	K-67	K-76
		($Wm^{-1} K^{-1}$)			(%)	(%)	(%)	(%)	(%)	(%)	(%)	(%)	(%)	(%)	(%)	(%)	(%)	(%)
	Quartz	7.20[1]	7.69[2]	7.99[1]	32.6	44.4	26.7	46.4	39.0	40.7	24.1	20.8	32.0	24.1	4.7	33.7	27.9	18.5
Plagioclase	**Albite**	2.00[3]	2.32[4]	2.35[3]	39.1	25.7	31.4	28.8	29.8	31.1	33.9	38.7	32.7	30.2	54.1	19.1	50.7	19.4
	Anorthite	1.54[3]	1.68[2]	1.90[5]	15.9	16.3	9.9	9.1	9.4	10.9	13.9	19.8	13.2	12.3	17.1	7.8	12.1	4.9
	Orthoclase	2.25[3]	2.32[6]	2.68[4]						2.5								1.3
K-Feldspar	**Orthoclase**	2.25[3]	2.32[6]	2.68[4]	2.2	1.3	7.0	4.4	3.6	1.0	6.2	9.5	6.1	11.1		26.1	4.0	43.5
	Albite	2.00[3]	2.32[4]	2.35[3]	0.2	0.1	0.8	0.8	0.4	0.1	0.6	1.1	0.6	1.2		2.8	0.4	2.3
Amphibole	**Hornblende**	2.54[2]	2.81[3]	3.08[3]	1.1										12.6[f]			
Opx	**Enstatite**	4.12[2]	4.16[a,3]	4.96[2]	2.7	2.7	6.4	1.0	6.3	0.9	6.0	4.2	0.9					
	Ferrosilite		4.16[a,3]		1.5	3.2	4.2	0.8	4.1	0.6	3.2	4.1	0.0	14.4				
Cpx	**Diopside**		4.06[3]	4.11[2]														
	Hedenbergite		3.82[b,3]															
	Clinoferrosilite		3.82[b,3]															
	Jadeite		4.62[3]	6.66[2]														
Garnet	**Almandine**		3.31[2]			2.8	5.4	3.1	2.8	2.1	1.3		4.4			3.9	1.4	2.9
	Pyrope		3.18[2]			1.7	4.3	2.5	2.2	1.4	1.0		3.6			3.2	1.1	3.0
	Grossular	5.12[2]	5.48[3]	5.64[2]		0.5												
Mica	**Biotite**	1.95[5]	2.02[3]	2.34[2]	4.0	1.2	4.0	3.1	1.7	8.7	9.8	1.2	6.6	5.2	5.0	3.1	2.3	4.2
	Phlogopite	1.963	2.13[3]	2.29[2]														
Others	**Illite**	1.85[7]	1.90[8]	2.00[9]														
	Ilmenite	2.19[2]	2.38[3]						0.6			0.9		1.6		0.3		
	Magnetite	5.10[2]	5.11[3]	5.84[3]	0.6													
	Epidote	2.62[2]	2.84[3]	3.03[3]											6.5			

[a] Considered TC of bronzite for ferrosilite, [b] considered TC of augite for hedenbergite and clinoferrosilite, [c] microcline with TC 2.49 (Horai, 1971), [d] maghemite, [e] pargasite, [f] magnesiohastingsite, Opx = orthopyroxene, Cpx = clinopyroxene. References: [1] Dortman (1976), [2] Horai and Simmons (1969), [3] Horai (1971), [4] Sass (1965), [5] Schön (1983), [6] Vasseur *et al.* (1995), 7 Brigaud and Vasseur (1989), [8] Hickox *et al.* (1986), [9] Čermák and Rybach (1982).

All samples display low porosities, ranging between 0.2 and 1.4% (Table 1). The low porosity is corroborated by the only small discrepancy (< 5 %) observed between measured dry and saturated TC values, which is within the analytical error. The low porosity is in line with previous estimations (Ray *et al.*, 2006), suggesting that microcracks and microporosity are of minor importance in our suite of samples.

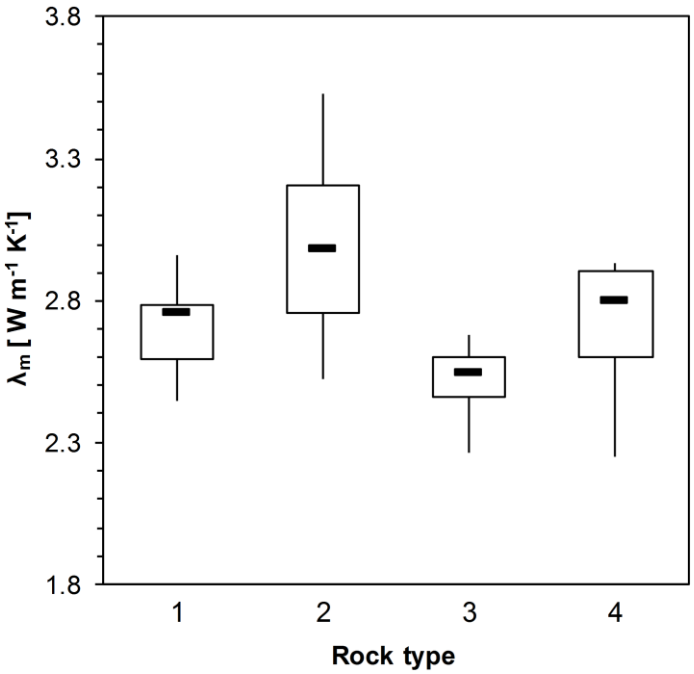

Figure 3 Means of bulk TC measured for different rock types (λm). For rock-type numbering and boxplot definition see Fig. 2.

4.2 Thermal conductivity calculated from mineral composition

The modal mineralogy/porosity of the rocks, along with the minimum, mean, and maximum TC values for individual mineral phases/end-members reported in the literature, are compiled in Table 2. The measured saturated bulk TC (λ_m) and the calculated bulk TC values (considering the mean values of mineral TC) exhibit the following ranking: $\lambda_m \sim \lambda_{HM} < \lambda^{L}_{HS} < \lambda_{Geo} < \lambda^{U}_{HS} \lambda_{eff} < \lambda_{AM}$. In this case, the harmonic mean provided by far the best approximation with the measured TC for either rock type (Table 3, Fig. 4). From a statistical point of view, application of this model results in significantly lower prediction errors compared to all other mixing models, with exception of the lower Hashin–Shtrikman boundary (ANOVA, Tukey HSD, α = 0.05). As to λ_{HM}, the deviations range between −11 and +16%. For 23 out of 26 samples, the deviation is > 10%. For the entire sample suite, the absolute deviation between λ *and* λ_{HM} averages to −1.2 ± 6.1% (1σ standard deviation).

Table 3 Measured saturated bulk TC (λ_m) versus saturated bulk TC calculated from mineralogical composition and porosity, adopting various mixing models.

TC ($Wm^{-1}K^{-1}$)	Charnockite							
	EK-105	**K-25**	**K-37**	**K-61**	**K-69**	**2-SK-2**	**KAN-3**	**NC-99**
Measured bulk TC								
λ_m	2.62	2.78	2.50	2.73	2.96	2.49	2.85	2.76
Calculated saturated bulk TC* (mean mineral TC values)								
λ_{HM}	2.62	2.72	2.58	2.84	2.82	2.63	2.78	2.72
λ_{AM}	3.62	3.64	3.34	4.01	3.91	3.53	4.03	3.89
λ_{GEO}	3.02	3.08	2.87	3.29	3.23	2.99	3.30	3.19
λ_{EFF}	3.16	3.24	2.99	3.49	3.47	3.10	3.45	3.39
λ^{L}_{HS}	3.00	3.07	2.86	3.27	3.21	2.98	3.26	3.16
λ^{U}_{HS}	3.35	3.43	3.14	3.75	3.69	3.28	3.70	3.63
Deviations (in %)								
λ_{HM}	**-0.4**	**-0.5**	**5.5**	**2.8**	**-6.3**	**5.8**	**-2.5**	**-2.8**
λ_{AM}	38.2	33.5	35.5	47.4	33.0	41.6	41.6	45.7
λ_{GEO}	15.5	13.7	17.3	21.3	10.4	19.9	15.8	19.9
λ_{EFF}	20.4	17.9	21.3	26.4	15.2	24.2	21.1	21.6
λ^{L}_{HS}	14.3	12.7	16.7	20.0	8.9	19.4	14.5	17.3
λ^{U}_{HS}	27.9	24.6	27.7	35.8	22.8	31.8	30.2	30.5
Calculated saturated bulk TC* (minimal mineral TC values)								
λ_{HM}	2.38	2.51	2.37	2.63	2.62	2.41	2.53	2.47
λ_{AM}	3.34	3.40	3.10	3.74	3.66	3.27	3.73	3.59
λ_{GEO}	2.76	2.85	2.65	3.06	3.02	2.75	3.02	2.90
λ_{EFF}	2.89	3.00	2.76	3.25	3.23	2.85	3.16	3.10
λ^{L}_{HS}	2.74	2.84	2.64	3.04	3.00	2.74	2.98	2.88
λ^{U}_{HS}	3.08	3.19	2.92	3.50	3.45	3.04	3.41	3.34
Deviations (in %)								
λ_{HM}	-9.1	-10.3	**-4.5**	**-4.6**	-12.7	**-2.0**	-12.3	-10.5
λ_{AM}	27.3	22.6	30.4	37.7	24.4	34.9	27.3	34.3
λ_{GEO}	5.4	3.1	9.4	12.9	3.0	12.2	3.7	8.1
λ_{EFF}	10.3	7.3	13.8	17.8	7.5	17.1	8.6	13.7
λ^{L}_{HS}	**4.5**	**2.2**	8.8	11.6	**1.6**	11.4	**2.6**	**6.7**
λ^{U}_{HS}	17.5	14.0	21.2	26.7	14.8	24.8	16.8	22.6
Calculated saturated bulk TC* (maximal mineral TC values)								
λ_{HM}	2.79	2.95	2.79	3.08	3.04	2.86	2.97	2.89
λ_{AM}	3.82	3.91	3.59	4.24	4.14	3.78	4.24	4.09
λ_{GEO}	3.22	3.33	3.11	3.53	3.47	3.24	3.51	3.37
λ_{EFF}	3.36	3.49	3.23	3.74	3.71	3.34	3.65	3.58
λ^{L}_{HS}	3.20	3.33	3.11	3.53	3.46	3.23	3.48	3.36
λ^{U}_{HS}	3.55	3.69	3.39	3.98	3.92	3.53	3.91	3.83
Deviations (in %)								
λ_{HM}	**8.2**	**4.5**	**11.0**	**11.6**	**1.0**	**15.8**	**0.0**	**7.6**
λ_{AM}	48.2	38.8	41.1	55.7	40.4	52.9	43.5	53.5
λ_{GEO}	24.9	18.8	22.5	30.1	18.1	31.3	18.5	26.8
λ_{EFF}	30.5	23.2	27.8	35.2	23.0	35.4	24.0	32.2
λ^{L}_{HS}	24.3	18.3	22.6	29.3	17.0	31.0	17.6	26.0
λ^{U}_{HS}	38.2	29.9	34.0	44.1	30.3	43.0	32.3	41.4

Continued

TC	Enderbite									
($Wm^{-1}K^{-1}$)	**98-46**	**KU-5**	**86**	**90**	**96**	**MP-98**	**MP-101**	**98-78**	**98-89A**	**K-71**
Measured bulk TC										
λ_m	2.75	3.52	3.01	3.52	3.15	3.22	2.96	2.53	2.79	2.66
Calculated saturated bulk TC* (mean mineral TC values)										
λ_{HM}	2.77	3.12	2.88	3.21	3.27	2.98	2.71	2.54	2.74	2.71
λ_{AM}	4.03	4.72	3.94	4.79	4.56	4.45	3.68	3.41	3.98	3.74
λ_{GEO}	3.30	3.88	3.34	3.95	3.83	3.64	3.10	2.86	3.27	3.14
λ_{EFF}	3.44	4.03	3.46	4.11	4.01	3.76	3.21	3.03	3.42	3.31
λ^{L}_{HS}	3.27	3.80	3.31	3.87	3.79	3.58	3.08	2.86	3.23	3.12
λ^{U}_{HS}	3.70	4.35	3.67	4.42	4.28	4.06	3.42	3.23	3.67	3.52
Deviations (in%)										
λ_{HM}	**1.0%**	-11.3	**-4.3**	**-8.7**	**3.1**	**-6.6**	-8.7	**-0.6**	**-1.9**	**0.8**
λ_{AM}	46.8	34.3	30.8	36.0	45.3	38.1	24.5	35.7	42.6	40.8
λ_{GEO}	20.0	10.1	10.9	12.3	22.2	13.1	4.7	14.2	17.3	18.2
λ_{EFF}	25.5	14.5	14.7	16.8	26.2	17.8	8.5	18.6	22.7	22.8
λ^{L}_{HS}	19.0	**8.2**	10.0	9.8	20.4	11.2	**4.0**	13.6	15.8	17.0
λ^{U}_{HS}	34.9	23.8	21.9	25.5	35.1	27.0	15.6	26.0	31.5	31.0
Calculated saturated bulk TC* (minimal mineral TC values)										
λ_{HM}	2.49	2.85	2.64	2.93	2.98	2.71	2.46	2.30	2.50	2.49
λ_{AM}	3.72	4.40	3.68	4.45	4.25	4.12	3.42	3.15	3.69	3.49
λ_{GEO}	3.00	3.57	3.09	3.63	3.53	3.34	2.84	2.61	3.00	2.90
λ_{EFF}	3.14	3.72	3.20	3.78	3.70	3.46	2.96	2.77	3.15	3.06
λ^{L}_{HS}	2.97	3.50	3.06	3.56	3.49	3.28	2.83	2.61	2.97	2.88
λ^{U}_{HS}	3.40	4.04	3.42	4.10	3.98	3.75	3.17	2.97	3.39	3.28
Deviations (in%)										
λ_{HM}	-9.4	-25.6	**-1.6**	-18.4	**-7.0**	-15.0	-16.7	-9.9	-10.2	**-7.4**
λ_{AM}	35.7	4.3	48.2	20.4	40.5	28.2	15.5	25.1	32.4	31.1
λ_{GEO}	9.5	-12.7	21.3	**-0.4**	14.8	3.7	-4.0	3.8	7.5	8.9
λ_{EFF}	14.2	-9.3	26.2	3.4	19.1	8.4	**-0.1**	8.3	12.8	13.6
λ^{L}_{HS}	**8.2**	-13.6	18.9	-2.2	12.9	**2.1**	-4.4	**3.4**	**6.3**	8.0
λ^{U}_{HS}	23.6	**-3.0**	36.6	11.4	29.6	17.5	7.0	15.8	21.5	21.5
Calculated saturated bulk TC* (maximal mineral TC values)										
λ_{HM}	2.94	3.31	3.07	3.38	3.47	3.17	2.91	2.72	2.91	2.93
λ_{AM}	4.24	4.95	4.17	4.99	4.81	4.65	3.92	3.63	4.16	4.03
λ_{GEO}	3.49	4.09	3.55	4.14	4.05	3.84	3.32	3.06	3.44	3.39
λ_{EFF}	3.63	4.25	3.67	4.30	4.24	3.96	3.44	3.24	3.60	3.57
λ^{L}_{HS}	3.47	4.04	3.53	4.08	4.03	3.79	3.32	3.07	3.42	3.39
λ^{U}_{HS}	3.90	4.58	3.90	4.62	4.52	4.26	3.65	3.44	3.84	3.79
Deviations (in%)										
λ_{HM}	**6.6**	-13.9	**11.9**	**-3.7**	**4.1**	**-1.0**	**-2.6**	**5.6**	**4.0**	**6.9**
λ_{AM}	53.6	16.1	65.4	34.6	56.3	44.2	29.9	41.7	49.0	46.7
λ_{GEO}	26.8	**-1.1**	37.0	13.6	29.3	18.9	10.4	20.1	23.2	24.2
λ_{EFF}	31.5	2.5	42.5	17.3	33.1	23.8	14.3	24.8	28.8	29.1
λ^{L}_{HS}	25.9	-1.6	35.0	12.6	27.3	17.8	10.3	20.0	22.3	23.5
λ^{U}_{HS}	40.9	8.5	52.9	25.2	43.4	32.9	21.2	32.1	37.5	36.7

Continued

TC ($Wm^{-1}K^{-1}$)	Mafic Granulite				Gneiss				Deviations	
	98-39	**306I**	**316I**	**KO2**	**98-43B**	**K-78**	**K-67**	**K-76**	**mean**	**1δSD**
Measured bulk TC										
λ_m	2.55	2.26	2.68	2.60	2.25	2.90	2.94	2.69		
Calculated saturated bulk TC* (mean mineral TC values)										
λ_{HM}	2.68	2.63	2.86	2.57	2.23	2.84	2.62	2.54		
λ_{AM}	3.35	3.01	3.77	2.83	2.52	4.08	3.72	3.29		
λ_{GEO}	2.93	2.81	3.28	2.69	2.35	3.36	3.07	2.83		
λ_{EFF}	3.09	2.85	3.39	2.73	2.39	3.54	3.21	2.94		
λ^{L}_{HS}	2.95	2.83	3.26	2.71	2.35	3.32	3.04	2.82		
λ^{U}_{HS}	3.27	2.95	3.59	2.81	2.45	3.78	3.43	3.08		
Deviations (in %)										
λ_{HM}	**3.4**	**16.4**	**6.6**	**-1.3**	**-1.0**	**-2.6**	-10.9	-5.7	**-1.2**	6.1
λ_{AM}	33.0	33.3	42.0	9.3	12.2	41.1	26.5	22.2	35.0	9.7
λ_{GEO}	16.3	24.6	23.4	4.0	4.8	16.4	4.2	5.4	14.5	6.2
λ_{EFF}	19.5	26.1	26.4	4.6	6.2	21.5	9.3	9.3	18.4	6.5
λ^{L}_{HS}	16.1	25.4	22.6	4.7	4.6	14.5	**3.2**	**4.8**	13.4	6.1
λ^{U}_{HS}	25.7	30.5	33.7	7.6	8.8	29.9	16.6	14.5	25.8	7.7
Calculated saturated bulk TC* (minimal mineral TC values)										
λ_{HM}	2.43	2.41	2.68	2.39	1.99	2.64	2.34	2.38		
λ_{AM}	3.12	2.85	3.59	2.69	2.25	3.82	3.40	3.09		
λ_{GEO}	2.68	2.62	3.10	2.53	2.09	3.14	2.76	2.66		
λ_{EFF}	2.84	2.66	3.21	2.57	2.13	3.30	2.90	2.76		
λ^{L}_{HS}	2.70	2.63	3.09	2.54	2.10	3.09	2.74	2.64		
λ^{U}_{HS}	3.03	2.77	3.42	2.66	2.18	3.54	3.12	2.90		
Deviations (in %)										
λ_{HM}	**-6.3**	**6.8**	**0.6**	-8.4	-11.7	-18.4	-10.2	-12.6	-9.5	6.6
λ_{AM}	23.6	26.5	34.4	3.9	**0.1**	6.4	30.2	26.5	25.8	11.7
λ_{GEO}	6.4	16.2	16.1	-2.3	-6.9	-8.5	7.2	2.8	5.4	8.0
λ_{EFF}	9.7	17.7	20.6	**-1.3**	-5.3	-5.1	11.9	8.0	9.6	8.5
λ^{L}_{HS}	6.3	16.7	15.7	-1.9	-6.8	-9.1	**5.5**	**1.9**	**4.5**	7.9
λ^{U}_{HS}	16.4	22.9	28.2	2.0	-2.9	**-0.4**	19.9	16.0	17.0	9.9
Calculated saturated bulk TC* (maximal mineral TC values)										
λ_{HM}	2.86	2.80	2.99	2.77	2.35	3.05	2.73	2.78		
λ_{AM}	3.63	3.20	3.88	3.09	2.65	4.30	3.86	3.53		
λ_{GEO}	3.15	2.99	3.40	2.92	2.48	3.59	3.20	3.09		
λ_{EFF}	3.33	3.03	3.52	2.96	2.52	3.77	3.35	3.19		
λ^{L}_{HS}	3.18	3.00	3.39	2.94	2.48	3.56	3.18	3.07		
λ^{U}_{HS}	3.52	3.13	3.70	3.05	2.58	4.01	3.56	3.33		
Deviations (in %)										
λ_{HM}	**7.7**	**23.7**	**8.8**	**1.5**	**4.4**	**-4.3**	**3.4**	**1.7**	**4.8**	7.3
λ_{AM}	36.4	41.0	41.0	11.3	17.7	21.8	46.7	43.6	41.2	13.1
λ_{GEO}	19.9	32.0	23.4	6.5	10.1	6.5	22.6	18.8	20.5	8.9
λ_{EFF}	23.2	33.4	27.2	7.3	12.1	10.1	27.8	24.4	24.8	9.4
λ^{L}_{HS}	20.1	32.7	22.9	7.1	10.3	6.0	21.2	18.2	19.9	8.6
λ^{U}_{HS}	29.2	37.8	33.7	9.9	14.5	14.8	35.8	32.4	32.0	10.9

λ_m: measured mean; λ_{HM}: harmonic mean; λ_{AM}: arithmetic mean; λ_{GEO}: geometric mean; λ_{EFF}: effective mean;
λ^{L}_{HS}, λ^{U}_{HS}: lower bound and upper bound of Hashin-Shtrikman mean; *Pore-filling fluid is water: TC_{water} = 0.605 $Wm^{-1}K^{-1}$.

The poorest fit between measured and calculated TC refers to the arithmetic mean (λ_{AM}), which consistently overestimates the measured TC, on average by 35 ± 10%. Application of all other mixing models evaluated in this study also yields an overestimation of TC between 13 and 26% (mean deviates, *cf.* Table 3).

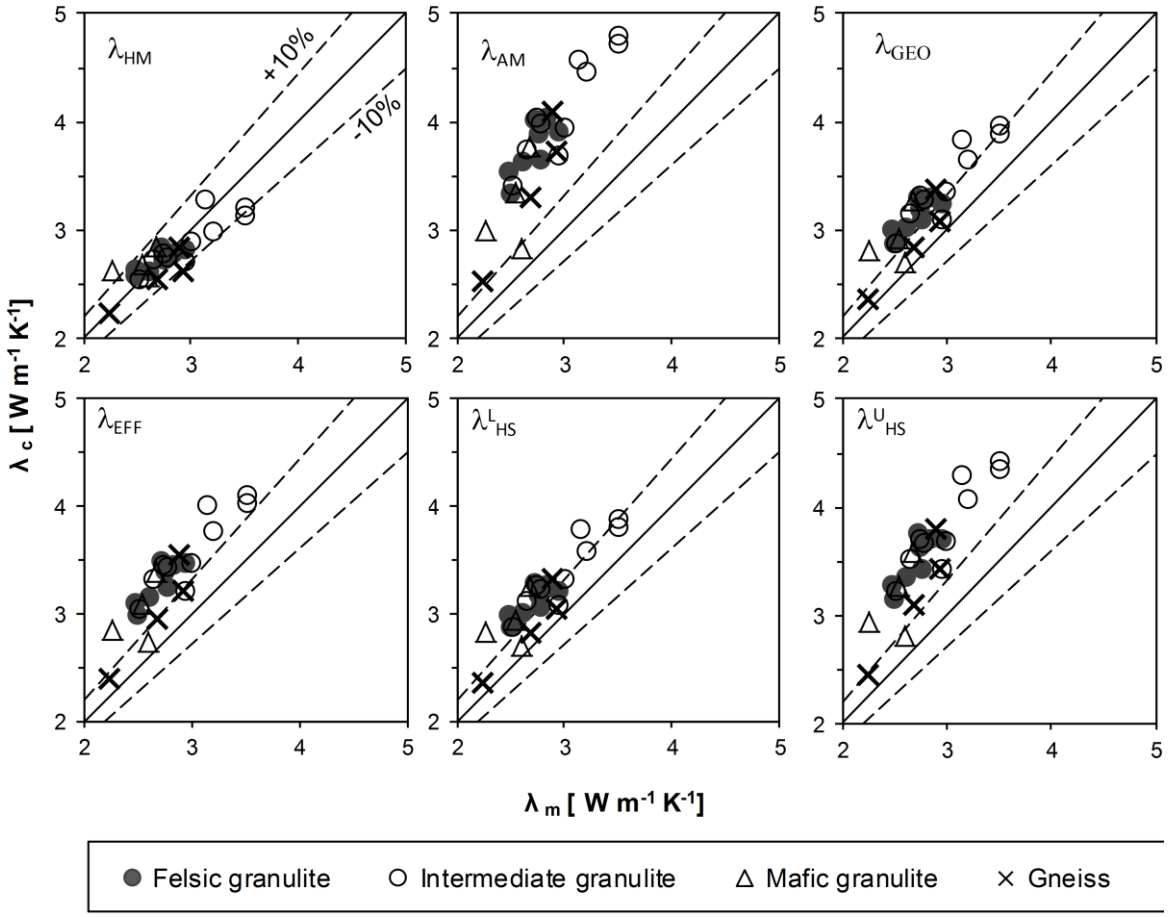

Figure 4 Scatter plots of calculated (λ_c) vs. measured (λ_m) bulk TC for different rock types and mixing models. λ_{HM}: harmonic mean; λ_{AM}: arithmetic mean; λ_{GEO}: geometric mean; λ^{L}_{HS}, λ^{U}_{HS}: lower bound and upper bound of Hashin-Shtrikman mean; λ_{EFF} : effective-medium mean.

5. Discussion

5.1 Thermal conductivity calculated from mineralogical composition

There is no study yet on granulite-facies rocks where TC is derived from their mineral assemblages. Corresponding studies were performed for igneous rocks (*e.g.*, Birch and Clark, 1940, Beck and Beck, 1965, Horai and Baldridge, 1972), amphibolite-facies metamorphic rocks (*e.g.*, Pribnow *et al.*, 1993; Pribnow and Umsonst, 1993) and sedimentary rocks (*e.g.*, Brigaud and Vasseur, 1989, Fuchs *et al.*, 2013). In most of these studies, the geometric mean, which takes no account of geometrical arrangement of minerals and pores, provided a variably good approximation to the values measured on none or only weakly textured rocks.

Correspondingly, the absence or weakness of any textural pattern in our suite of samples should also call for the application of a mixing model that does not consider any layering of minerals or pores in the rock, and this logically would be the geometric mean model. Unexpectedly, consideration of mean values of mineral TC resulted in a continuous underestimation of the measured TC with the geometric mean model by 15 ± 6%. Even more puzzling is the fact that the harmonic mean shows the smallest average absolute deviation (−1.2 ± 6.1) followed by the lower bound of the Hashin–Shtrikman mean (13.4 ± 6.1%), both being theoretically representative for a layered arrangement of minerals or pores.

The observed paradox in the ranking of the mixing model results could be resolved, if the data set is investigated for its sensitivity due to variation in mineral TC. Particularly quartz, feldspars and pyroxenes display some TC anisotropy in rock, which also is reflected in laboratory measurements of rock samples (Birch and Clark, 1940; Diment, 1964; Sass, 1965; Hofer and Schilling, 2002). Indeed, the application of minimal mineral TC values yields a different prediction performance (*cf.* Table 3, Fig. 5). Here, the best approximation to measured TC is by the lower Hashin-Shtrikman boundary (absolute deviations: 4.5 ± 7.9%) and by the geometric mean model (absolute deviations: 5.4 ± 8.9%). The harmonic mean model also provides a relatively good fit, but tends to underestimate the measured bulk TC (−9.5 ± 6.6). In contrast, for maximum TC of individual minerals (*cf.* Table 2), the harmonic-mean model again displays significantly lower prediction errors compared to all other mixing model results (Table 3). The absolute deviation between λ_m and λ_{HM} averages to 7.4 ± 5.0%. Differences in prediction capability between λ_{HS}^{L}, λ_{Geo}, and λ_{eff} are in the range 20−25%.

Reasons for the observed discrepancies between measured and calculated bulk thermal conductivity are numerous. Analytical and measurement errors, however, appear only being of secondary importance. These differences may as well result to some part from the physical-mathematical formulations of the evaluated mixing models, which describe in a rather simple manner the real, likely more complicated nature of a rock. The most crucial parameter is ambiguity in the knowledge of mineral TC. Depending on which TC value is used for a particular mineral (this particularly applies to quartz, feldspars and pyroxenes in our suite of samples), different mean models of partly different physical rationale provide the best fits to the measured TC. Future work is demanded to resolve this ambiguity.

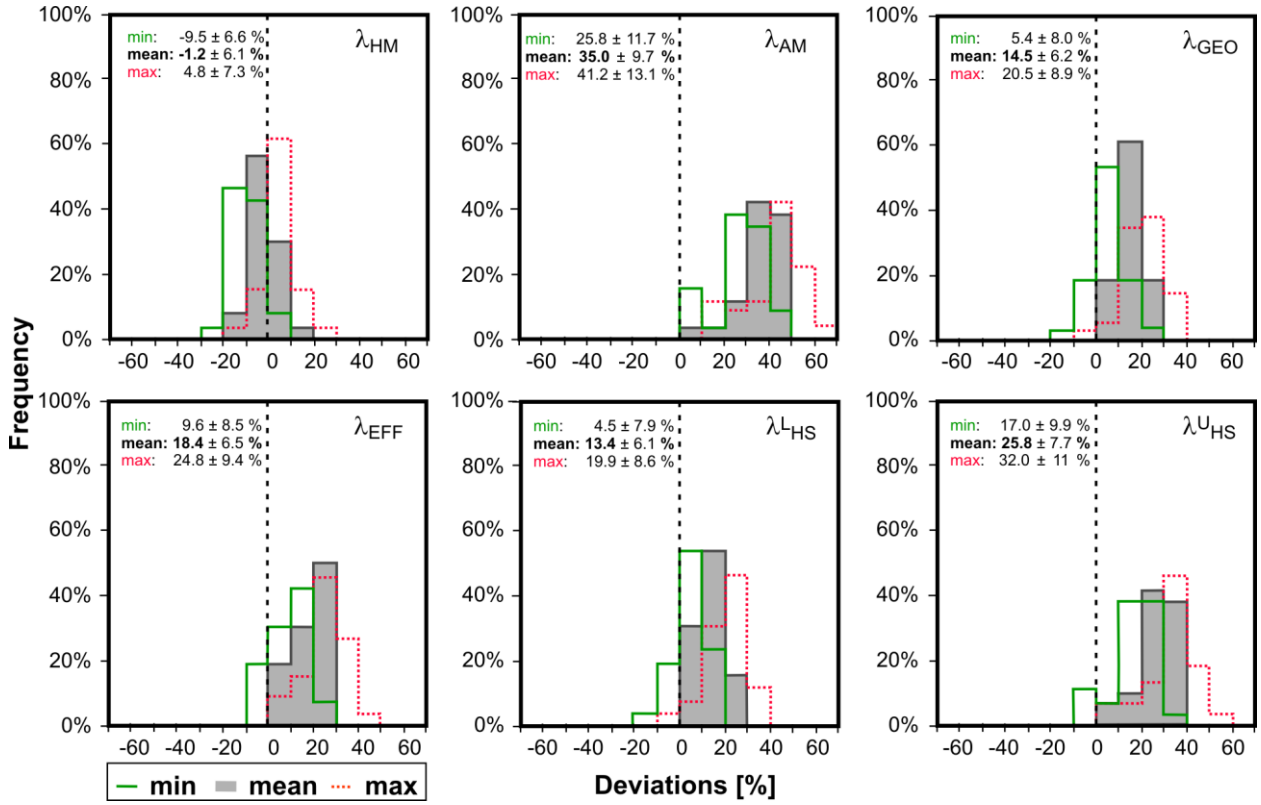

Figure 5: Bar diagram showing the deviations between measured and calculated bulk TC (saturated) for different mixing models. Calculation is based on minimum (solid green bar borders), mean (grey shaded bar borders) and maximum (dotted red bar borders) mineral TC values listed in Table 3.Bar diagram showing the deviations between measured and calculated bulk TC (saturated) for different mixing models. Calculation is based on minimum (solid green bar borders), mean (grey shaded bar borders) and maximum (dotted red bar borders) mineral TC.

5.2 Thermal conductivity of the continental lower crust

Previous comprehensive TC studies of metamorphic rocks from the Southern Granulite Province, India (Ray, 2002; Ray *et al.*, 2003; Roy *et al.*, 2003, 2007) (i) did not distinguish between felsic granulites (charnockites) and intermediate granulites (enderbites) (collectively referred to as charnockites), (ii) did not include mafic granulites and (iii) lacked a detailed mineralogical and geochemical characterization of the samples. Merging the values from these studies with the data presented here, felsic and intermediate granulites from this province display a relatively large range in TC, with values between 2.0 and 3.5 W m^{-1} K^{-1}. The TC of mafic granulites spans a much narrower range, *i.e.*, between 2.4 and 2.7 W m^{-1} K^{-1}.

Worldwide, a poor database is available for felsic and intermediate granulites. The TC of charnockites from the Limpopo Belt in southern Africa averaged to 2.8 W m^{-1} K^{-1} (Nyblade *et al.*, 1990), which is in close correspondence with the respective data from this study. Two enderbite samples from Fennoscandia studied by Kukkonen *et al.* (1999) yielded TC values of 2.1 and 2.3 W m^{-1} K^{-1}, respectively, which are considerably lower than those presented here for this rock type.

Regarding mafic granulites, which are the typical components of the lower continental crust (*cf.* Rudnick and Fountain, 1995; Furlong and Chapman, 2013), our TC values largely coincide with data reported from other granulite terranes. Measured TC values range between 2.1 and 2.5 W m^{-1} K^{-1} for mafic granulites from the central Fennoscandian Shield in Finland (Kukkonen *et al.*, 1999). Pyroxene granulites from the Fraser Range in Australia have an average TC of 2.4 ± 0.07 W m^{-1} K^{-1} (Jaeger, 1970). Average value of pyroxene and garnet-bearing granulites from the Saxon Granulite Massif (Germany) is 2.6 W m^{-1} K^{-1} (Seipold, 1992). Slightly larger values of 2.8–3.0 W m^{-1} K^{-1} were determined for mafic granulites from the Arabian Shield in Jordan (Förster *et al.*, 2010). Calculation of bulk TC (using λ_{HM} and mean TCs for minerals) for a suite of partially re-equilibrated, weakly porous (porosity: 3–8 %) and microcrack-penetrated mafic granulites from the northern Arabian Shield in Israel studied by Schütz *et al.* (2014), which contain feldspars, pyroxenes, and garnets in variable proportions and, thus, are representative for a wide range of compositions typifying the lower crust, yielded values between 2.5 and 3.2 W m^{-1} K^{-1}.

Joeleht and Kukkonen (1998) measured 252 samples from five granulite-facies terranes in Finland and Estonia. The authors reported comparatively high mean TC values varying between 3.0 and 3.5 W m^{-1} K^{-1}, which they attributed to uncommonly high modal abundances of sillimanite and quartz in a variety of samples. Moreover, the suite of studied rocks contains, among others, granulites of sedimentary origin and such that have intermediate and silicic volcanic rocks as precursors, all of which are unusual components of the lower crust.

If we consider mafic granulites as typical constituents of the lower crust, at ambient temperature and pressure conditions, the TC of rocks from this part of the continental lithosphere normally span the range 2 to 3 W m^{-1} K^{-1}, with the bulk of available data concentrated in the interval 2.5 to 3.0 W m^{-1} K^{-1}. In case those samples are unavailable for direct measurement or calculation of TC from mineral composition, any modeling of the thermal structure of a crustal segment must take this potential range into consideration.

Acknowledgements

Experimental and analytical works were performed at Deutsches GeoForschungsZentrum GFZ, Potsdam (Germany), and we wish to thank all the staff members, who supported or supervised these parts of the study. F. Schütz (Berlin) kindly provided petrophysical and mineralogical data for thermal conductivity calculation from modal mineralogy of lower-crustal xenoliths from Israel. I. Braun and M. Raith (Bonn) are thanked for providing samples (86, 90, 96, KU5, KO2, 306I and 316I). Y. Guéguen (Paris) offered valuable comments on an earlier draft that

helped to improve this paper. Two anonymous reviewers offered valuable comments, which helped to strengthen the paper. LR is supported by SHORE (PSC-0205) project funded by CSIR. LR is indebted to R.U.M. Rao (India) for incessant encouragement and valuable suggestions in different stages of work and to Director CSIR-NGRI, for his support.

References

Abdulagatova, Z.Z., Abdulagatov, I.M., Emirov, S.N., 2009. Effect of temperature and pressure on the thermal conductivity of sandstone. International Journal of Rock Mechanics and Mining Sciences 46, 1,055–1,071.

Beck, J.M., Beck, A.E., 1965. Computing thermal conductivities of rocks from chips and conventional specimens. Journal of Geophysical Research B70, 5,227–5,239.

Bergmann, J., Friedel. P. Kleeberg. R., 1998. BGMN: a new fundamental parameters based Rietveld program for laboratory X-ray sources, its use in quantitative analysis and structure investigations. Continuing Professional Development Newsletter 20, 5–8.

Birch, F., 1950. Flow of heat in the Front Range, Colorado. Geological Society of America Bulletin 61, 567–630.

Birch, F., Clark, H., 1940. The thermal conductivity of rocks and its dependence upon temperature and composition. American Journal of Science 238, 529–635.

Brigaud, F., Vasseur, G., 1989. Mineralogy, porosity and fluid control on thermal conductivity of sedimentary rocks, Geophysical Journal International 98, 525–542.

Bruggeman, D.A.G., 1935. Berechnung verschiedener Konstanten von heterogenen Substanzen – I. Dielektrizitätskonstanten und Leitfähigkeiten der Mischkörper aus isotropen Substanzen. Annals of Physics 24, 636–679.

Bullard, E.C., 1939. Heat flow in South Africa. Proceedings of the Royal Society A173, 474–502.

Carslaw, H., Jaeger, J.C., 1947. Conduction of Heat in Solids. Oxford, Clarendon.

Čermák, V., Rybach, L., 1982. Thermal properties. In: Hellwege, K.-H. (Ed.), Landolt-Bornstein Numerical Data and Functional Relationships in Science and Technology, New Series, Group V. Geophysics and Space Research, vol. 1, Physical Properties of Rocks, subvol. A. Springer, Berlin, pp. 305–371.

Diment, W.H., 1964. Thermal conductivity of serpentinite from Mayaguez, Puerto Rico, and other localities. National Academy of Sciences−National Research Council Publication 1188, 92–106.

Dortman, N.B., 1976. Fiziceskie Svoistva Gornich Porod i Polesnich Iskopaemych. Izdat Nedra, Moskva.

Förster, H.-J., Tischendorf, G., Trumbull, R.B., Gottesmann, B., 1999. Late-collisional granites in the Variscan Erzgebirge, Germany. Journal of Petrology 40, 1,613–1,645.

Förster, H.-J., Förster, A., Oberhänsli, R., Stromeyer, D., 2010. Lithospheric composition and thermal structure of the Arabian Shield in Jordan. Tectonophysics 481, 29–37.

Förster, A., Förster, H.-J., Masarweh, R., Masri, A., Tarawneh, K., 2007. The surface heat flow of the Arabian Shield in Jordan. Journal Asian Earth Sciences 30, 271–284.

Fuchs, S., Schütz, F., Förster, H.-J., Förster, A., 2013. Evaluation of common mixing models for calculating bulk thermal conductivity of sedimentary rocks: correction charts and new conversion equations. Geothermics 47, 40–52.

Furlong, K.P., Chapman, D.S., 2013. Heat flow, heat generation, and the thermal state of the lithosphere. Annual Review of Earth and Planetary Sciences 41, 385–410.

Geological Map of India, 1998. Geological Survey of India. 7th Edition, 1:2,000,000.

Gopalkrishna, D., Hansen, E.C., Janardhan, A.S., Newton, R.C., 1986. The southern high-grade margin of the Dharwar craton. Journal of Geology 94, 247–260.

Hashin Z., Shtrikman, S., 1962. A variational approach to the theory of the effective magnetic permeability of multiphase materials, Journal of Applied Physics 33, 3,125–3,131.

Hickox, C.E., McVey, D.F., Miller, J.B., Olson, L.O. Silva, A.J., 1986. Thermal conductivity measurements of Pacific illite sediments. International Journal of Thermophysics 7, 755–764.

Hofer, M., Schilling, F.R. 2002. Heat transfer in quartz, orthoclase, and sanidine at elevated temperature. Physics and Chemistry of Minerals 29, 571–584.

Horai, K.-I., 1971. Thermal conductivity of rock-forming minerals. Journal of Geophysical Research B76, 1,278–1,308.

Horai K.-I., Baldridge, S., 1972. Thermal conductivity of nineteen igneous rocks. II Estimation of the thermal conductivity of rock from the mineral and chemical compositions. Physics of the Earth and Planetary Interior 5, 157–166.

Horai, K.-I., Simmons, G., 1969. Thermal conductivity of rock-forming minerals. Earth and Planetary Science Letters 6, 359–368.

Jaeger, J.C., 1958. The measurement of thermal conductivity and diffusivity with cylindrical probes, EOS Transactions American Geophysical Union 39, 708–710.

Jaeger, J.C., 1970. Heat flow and radioactivity in Australia. Earth and Planetary Science Letters 8, 285–292.

Joeleht, A., Kukkonen, I.T., 1998. Thermal properties of granulite facies rocks in the Precambrian basement of Finland and Estonia. Tectonophysics 291, 195–203.

Jessop, A.M., 2013. Thermal conductivity of short rock sequences. International Journal of Earth Sciences 102, 483–491.

Kukkonen, I.T., Jokinen, J., Seipold, U., 1999. Temperature and pressure dependencies of thermal transport properties of rocks: Implications for uncertainties in thermal lithosphere models and new laboratory measurements of high-grade rocks in the Central Fennoscandian Shield. Surveys in Geophysics 20, 33–59.

Lichtenecker, K., 1924. Der elektrische Leitungswiderstand künstlicher und natürlicher Aggregate, Physikalische Zeitschrift 25, 169−181, 193−204, 226−233.

Nyblade, A.A., Pollack, H.N., Jones, D.L., Podmore, F., Mushayandebvu, M., 1990. Terrestrial heat flow in East and Southern Africa. Journal of Geophysical Research B95, 17,371–17,384.

Popov, Y.A., Pribnow, D.F.C., Sass, J.H., Williams, C.F., Burkhardt, H., 1999. Characterization of rock thermal conductivity by high-resolution optical scanning. Geothermics 28, 253–276.

Pribnow, D., Umsonst, T., 1993. Estimation of thermal conductivity from the mineral composition: Influence of fabric and anisotropy. Geophysical Research Letter 20, 199–202.

Pribnow, D., Williams, C., Burkhardt, H., 1993. Log-derived estimate for thermal conductivity of crystalline rocks from the 4 km KTB Vorbohrung. Geophysical Research Letters 20, 1,155–1,158.

Ray, L., 2002. Crustal thermal structure of the Southern Granulite Province, India. PhD thesis, Osmania University, Hyderabad.

Ray, L., Förster, H.-J., Schilling, F.R., Förster, A., 2006. Thermal diffusivity of felsic to mafic granulites at elevated temperatures. Earth and Planetary Science Letters 7, 241–253.

Ray, L., Senthil Kumar, P., Reddy, G.K., Roy, S., Rao, G.V., Srinivasan, R., Rao, R.U.M., 2003. High mantle heat flow in a Precambrian granulite province: Evidence from Southern India. Journal of Geophysical Research 108(B2) 2084 doi: 10.1029/ 2001JB000688.

Reuss, A., 1929. Berechnung der Fließgrenze von Mischkristallen auf Grund von Plastizitätsbedingung für Einkristalle. Zeitschrift für Angewandte Mathematik und Mechanik 9, 49–58.

Roy, S., Ray, L., Senthil Kumar, P., Reddy, G.K., Srinivasan, R., 2003. Heat flow and heat production in the Precambrian gneiss–granulite province of Southern India. Memoir Geological Society India No. 50, 177–191.

Roy, S., Ray, L., Bhatteracharya, A., Srinivasan, R., 2007. New heat flow data from deep boreholes in the greenstone–granite-gneiss and gneiss–granulite provinces of southern India, Department of Science and Technology Newsletter 17, 8–11.

Rudnick, R.L., Fountain, D.M., 1995. Nature and composition of the continental crust: a lower crustal perspective, Reviews of Geophysics 33, 267–309.

Sass, J.H., 1965. The thermal conductivity of fifteen feldspar specimens. Journal of Geophysical Research B70, 4,064–4,065.

Schön, J., 1983. Petrophysik. Akademie-Verlag, Berlin, 405 pp.

Schütz, F., Förster, H.-J., Förster, A., 2014. Thermal conditions of the northern Sinai Microplate inferred from new surface heat-flow values and continuous borehole temperature logging in central and southern Israel. Journal of Geodynamics 76, 8–24.

Seipold, U., 1992. Depth dependence of thermal transport properties for typical crustal rocks. Physics of the Earth and Planetary Interior 69, 299–303.

Vasseur, G., Brigaud, F., Demongodin, L., 1995. Thermal conductivity estimation in sedimentary basins. Tectonophysics 244, 167–174.

Voigt, W., 1928. Lehrbuch der Kristallphysik. Teubner, Leipzig.

Wiener, O.H., 1912. Die Theorie des Mischkörpers für das Feld der stationären Strömung, Erste Abhandlung: Die Mittelwertsätze für Kraft, Polarisation und Energie, Abh. math.-phys. Klasse Königlich-Sächsischen Ges. Wiss. 32, 507–604.

Appendix Whole-rock geochemistry

Rock type	Charnockite								Mafic granulite			
Sample no.	EK-105	K-25	K-37	K-61	K-69	2-SK-2	KAN-3	NC-99	98-39	306I	316I	KO2
SiO_2 (wt%)	67.9	68.3	64.2	65.3	65.3	65.2	70.5	69.5	57.2	50.8	55.8	47.0
TiO_2	0.59	0.45	0.72	1.08	0.80	0.43	0.36	0.45	1.15	0.75	0.59	0.80
Al_2O_3	14.5	13.9	15.2	14.1	15.0	15.3	14.9	14.8	15.8	14.7	13.2	16.3
Fe_2O_3[a]	4.37	4.34	6.12	7.79	6.57	4.83	2.23	3.61	11.2	11.5	11.2	12.7
MnO	0.06	0.11	0.10	0.09	0.08	0.08	0.02	0.04	0.16	0.18	0.20	0.19
MgO	0.58	1.73	0.45	1.27	0.90	1.84	0.73	0.70	5.27	6.32	6.36	8.09
CaO	2.60	2.12	2.53	2.80	2.59	3.86	2.65	2.83	3.45	11.2	9.56	11.4
Na_2O	3.57	2.58	3.16	2.27	2.00	2.95	3.53	3.98	3.82	3.14	1.82	1.94
K_2O	4.43	5.15	5.96	3.91	5.41	3.87	2.90	2.76	1.02	0.51	0.21	0.51
P_2O_5	0.19	0.14	0.16	0.24	0.35	0.20	0.05	0.14	0.02	0.07	0.07	0.06
H_2O^+	0.70	0.52	0.69	0.50	0.47	0.69	0.43	0.58	0.62	0.64	0.59	0.74
CO_2	0.28	0.28	0.44	0.18	0.29	0.43	0.05	0.37	0.04	0.10	0.40	0.37
Total	99.8	99.6	99.8	99.6	99.8	99.6	99.8	99.7	99.8	100.0	100.1	100.1
									36	39	38	44
Sc (ppm)	15		12	22	19		<10	10	253	253	251	296
V	26	57	<10	61	21	88	27	28	553	216	56	207
Cr	<10	59	<10	147	134	54	131	119	210	118	75	106
Ni	<10	17	<10	13	12	22	11	<10	137	101	56	73
Zn	73	57	107	83	83	67	28	52	22	18	14	15
Ga	19	17	19	17	17	18	15	22	10	1.8	1.1	1.3
Rb	93	149	131	197	183	124	55	61	405	211	98	169
Sr	284	476	270	105	146	762	498	603	8.6	26.5	21.3	19.8
Y	47.5	25.0	35.8	52.9	93.5	76.0	1.1	7.1	105	53	70	33
Zr	496	396	713	462	533	179	139	386	14.0	3.5	2.4	1.8
Nb	20	<10	22	19	33	<10	2.2	10.0	0.01	<0.006	<0.006	<0.006
Cs	0.17		0.17	0.87	0.45		0.03	0.03	755	163	61	48
Ba	1752	1805	2735	880	1194	1965	941	862	18.3	15.8	10.2	2.8
La	39.6		49.1	71.0	117		68.8	57.9	26.3	43.4	21.9	7.4
Ce	88.7		100	139	237		103	99.0	2.35	6.36	2.70	1.16
Pr	11.7		12.1	15.6	27.4		8.89	10.2	7.31	28.0	10.6	5.8
Nd	49.3		49.7	57.4	103		25.3	35.8	1.09	6.25	2.55	1.87
Sm	11.2		10.0	10.8	18.9		1.86	4.95	1.02	1.45	0.73	0.78
Eu	3.42		4.39	1.32	1.96		1.85	1.86	1.30	5.68	3.09	2.72
Gd	10.4		8.60	10.8	16.7		0.70	3.05	0.22	0.88	0.55	0.50
Tb	1.60		1.28	1.66	2.53		0.06	0.34	1.53	5.20	3.68	3.44
Dy	9.56		7.43	10.1	16.2		0.23	1.65	0.34	1.05	0.80	0.78
Ho	1.91		1.43	2.00	3.52		0.04	0.27	1.06	2.86	2.40	2.33
Er	5.34		3.99	5.65	10.5		0.13	0.68	0.15	0.40	0.36	0.36
Tm	0.74		0.56	0.78	1.52		0.02	0.09	1.11	2.43	2.43	2.31
Yb	4.68		3.57	4.99	9.71		0.15	0.56	0.20	0.36	0.38	0.36
Lu	0.70		0.57	0.73	1.40		0.03	0.09	3.0	1.8	1.9	1.0
Hf	10.9		14.9	11.9	13.1		3.6	8.0	0.52	0.14	0.22	0.08
Ta	0.88		0.77	0.82	1.9		0.05	0.34	8.9	3.5	3.9	2.7
Pb	22.0		20.4	25.7	41.5		11.0	18.0	0.15	0.28	2.9	<0.06
Th	1.56		1.3	3.0	25.7		5.4	0.41	0.13	0.04	1.2	0.02
U	0.38		0.28	0.30	0.51		0.18	0.73	**98-39**	**306I**	**316I**	**KO2**

Rock type	Enderbite										Gneiss			
Sample No.	**98-46**	**KU-5**	**86**	**90**	**96**	**MP-98**	**MP-101**	**98-78**	**98-89A**	**K-71**	**98-43B**	**K-78**	**K-67**	**K-76**
SiO_2 (wt%)	65.5	70.7	61.9	70.5	68.8	69.8	61.3	59.7	63.8	62.8	55.7	68.1	68.8	63.9
TiO_2	0.63	0.42	0.63	0.54	0.56	0.48	0.75	0.95	0.86	1.18	0.67	0.75	0.44	0.69
Al_2O_3	14.8	12.7	14.9	12.7	12.5	13.9	14.9	17.1	15.8	14.6	20.2	14.5	16.9	16.0
Fe_2O_3[a]	5.65	5.77	9.43	5.49	7.60	5.08	8.99	7.54	7.34	7.70	5.03	5.61	2.49	4.98
MnO	0.06	0.10	0.11	0.06	0.09	0.06	0.07	0.08	0.08	0.11	0.06	0.08	0.01	0.06
MgO	2.37	2.24	4.01	2.65	3.19	2.24	4.25	2.81	2.81	3.63	2.76	0.86	0.94	1.20
CaO	4.33	3.76	3.04	2.72	2.67	2.84	3.03	4.88	4.88	3.70	7.07	2.13	3.12	1.87
Na_2O	3.87	2.66	2.80	2.30	2.88	3.22	3.13	3.95	3.95	2.74	5.61	2.21	4.73	1.93
K_2O	0.95	0.37	1.44	1.38	0.80	1.37	2.19	1.70	1.70	2.26	1.14	4.69	1.66	7.49
P_2O_5	0.21	0.12	0.14	0.03	0.07	0.10	0.05	0.29	0.29	0.25	0.22	0.31	0.07	0.55
H_2O^+	0.61	0.50	0.76	0.71	0.53	0.91	0.78	0.55	0.55	0.45	0.78	0.72	0.69	0.87
CO_2	0.73	0.57	0.59	0.50	0.13	0.11	0.32	0.17	0.17	0.20	0.35	0.11	0.14	0.13
Total	99.8	99.9	99.7	99.6	99.8	100.1	99.7	99.8	99.8	99.6	99.7	100.1	100.0	99.7
Sc (ppm)	17	13				17	22	19	22	23	20	14	11	12
V	96	76	141	100	119	87	149	79	108	145	94	18	48	23
Cr	209	118	180	220	164	107	278	124	231	165	125	22	28	31
Ni	70	54	85	95	69	49	96	23	75	60	28	10	13	12
Zn	66	66	96	72	88	58	121	119	82	110	54	68	57	59
Ga	16	15	16	16	15	18	17	20	18	14	23	18	22	18
Rb	4.0	1.8	43	69	29	40	65	67	56	81	5.7	203	62	340
Sr	550	169	273	210	188	219	251	303	360	476	1059	115	612	135
Y	7.6	16.9	29	19	19	15.6	7.2	14.6	25.3	20.0	15.1	66.2	5.9	48.5
Zr	160	111	136	96	137	167	133	151	163	238	381	375	133	479
Nb	3.7	4.9	<10	<10	<10	5.5	8.6	9.0	13.2	11.5	5.3	21.9	9.4	17.3
Cs	<0.006	<0.006				0.19	0.31	0.30	0.25	1.61	0.01	1.46	0.13	1.15
Ba	550	157	445	273	217	301	560	422	485	1185	315	933	338	1056
La	26.7	20.8				34.0	42.1	30.0	28.6	55.5	30.1	97.0	21.3	160
Ce	46.9	40.4				62.8	73.9	66.0	59.1	109	59.8	194	41.5	347
Pr	5.18	4.56				6.76	7.53	8.07	7.13	12.3	7.31	21.9	4.53	40.4
Nd	19.6	16.9				24.4	25.0	31.2	28.3	46.2	29.3	80.8	16.2	150
Sm	3.04	3.35				4.10	3.13	5.84	5.95	7.78	5.49	14.8	2.90	28.1
Eu	1.01	0.83				1.01	1.14	1.49	1.39	2.04	1.86	1.31	1.05	1.64
Gd	2.32	3.16				3.28	1.95	4.77	5.40	6.19	4.32	12.7	2.08	19.8
Tb	0.29	0.49				0.48	0.24	0.61	0.82	0.78	0.55	1.98	0.26	2.31
Dy	1.55	3.00				2.84	1.35	3.24	4.94	4.29	3.05	12.1	1.33	10.9
Ho	0.29	0.61				0.58	0.26	0.58	0.97	0.78	0.58	2.50	0.23	1.92
Er	0.77	1.86				1.71	0.80	1.47	2.73	2.10	1.56	7.06	0.49	4.85
Tm	0.11	0.29				0.25	0.12	0.19	0.39	0.30	0.20	0.99	0.05	0.64
Yb	0.63	2.12				1.62	0.85	1.09	2.50	1.89	1.27	6.11	0.23	3.97
Lu	0.09	0.35				0.25	0.14	0.16	0.37	0.29	0.19	0.89	0.04	0.61
Hf	4.0	2.9				4.1	3.3	3.3	4.0	5.9	8.0	9.5	3.2	13.1
Ta	0.09	0.48				0.34	0.40	0.57	0.78	0.41	0.18	1.2	0.37	0.77
Pb	6.34	8.08				14.2	18.1	9.9	12.1	11.9	10.7	36.6	20.9	46.7
Th	0.11	5.19				12.3	16.0	0.73	2.8	12.4	0.34	29.9	1.58	82.2
U	0.18	3.08				1.25	0.74	0.19	0.56	0.85	0.07	2.3	0.22	4.73

Notes: [a] – total iron as Fe_2O_3.